Ab Initio Prediction of Vibrational Absorption and Circular Dichroism Spectra of Chiral Natural Products Using Density Functional Theory: Camphor and Fenchone

F. J. Devlin and P. J. Stephens*

Department of Chemistry, University of Southern California, Los Angeles, California 90089-0482

J. R. Cheeseman and M. J. Frisch

Lorentzian Inc., 140 Washington Avenue, North Haven, Connecticut 06473

Received: April 8, 1997[⊗]

Density functional theory (DFT) is used to assign the vibrational unpolarized absorption and circular dichroism spectra of two monoterpenes: camphor and fenchone. Calculations are carried out using the hybrid functionals B3PW91 and B3LYP at the TZ2P and 6-31G* basis set levels using direct analytical derivative methods and (for the calculation of atomic axial tensors) GIAOs. B3PW91/TZ2P calculations are in best agreement with experiment and provide the most convincing assignment of the spectra.

Introduction

We report calculations of the fundamental vibrational unpolarised absorption and circular dichroism spectra of two chiral monoterpene natural products using density functional theory (DFT). Recent developments permit vibrational absorption and circular dichroism spectra to be predicted using DFT both more accurately and more efficiently than heretofore.[1,2] Here, we exploit these developments in analyzing the vibrational spectra of camphor (**1**) and fenchone (**2**).

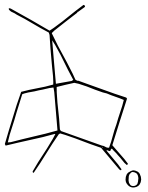

(1R,4R)-(+)-**1**

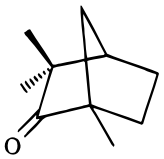

(1S,4S)-(+)-**2**

Camphor and fenchone are chosen for this study for several reasons. First, their vibrational circular dichroism (VCD) spectra have been reported over a substantial fraction of the fundamental vibrational infrared spectral region.[3−13] Simultaneous comparison of theory and experiment for both unpolarized absorption and VCD spectra is therefore possible. Second, their size leads to vibrational spectra of considerable complexity, providing a substantial challenge to theory. Third, they are conformationally rigid, so that the complexity resulting from conformational multiplicity is avoided. Last, prior analysis of these vibrational spectra is very limited.[14,15]

The prediction of absorption and VCD spectra within the harmonic approximation requires the calculation of harmonic frequencies, dipole strengths and rotational strengths. These in turn require calculation of the molecular Hessian (Cartesian harmonic force field), atomic polar tensors (APTs), and atomic axial tensors (AATs).[15−18] Several recent developments have enormously enhanced the accuracy and efficiency of DFT calculations of these properties. Most important are the implementation of direct analytical derivative methods for calculating all three properties,[1,19,20] the incorporation of gauge invariant (including) atomic orbitals (GIAOs) in the calculation of AATs,[1] and the development of hybrid density functionals.[21,22] In the present work, we take advantage of these developments in carrying out calculations for camphor and fenchone. Two currently available hybrid density functionals are employed and their relative accuracies assessed. Both medium-sized and large basis sets are used to define the basis set dependence of predicted spectra.

Preliminary results were communicated previously.[23]

Methods

Unpolarized absorption spectra of **1** and **2** were measured at 1 cm^{-1} resolution in CCl_4 and CS_2 solutions using a Nicolet MX-1 FTIR spectrometer. (1*R*,4*R*)-(+)- **1** and (1*S*,4*S*)-(+)- **2** were obtained from Aldrich and Fluka, respectively, and were used without further purification. The specified purities were 99% and >98%, respectively. Specific rotations were $[\alpha]_D^{25} = +44.1°$ ($c = 10$, C_2H_5OH) and $[\alpha]_D^{20} = +60°$ (neat), respectively. CCl_4 and CS_2 solvents were from EMScience and Fisher Scientific, respectively. KBr cells of 44 and 258 μm path (International Crystal Labs, Inc.) were used.

Mid-IR VCD spectra of (1*R*,4*R*)-(+)-**1** and (1*S*,4*S*)-(+)-**2** were taken from the literature.[9,11] For both **1** and **2** CCl_4 solutions were used; spectral resolution was 4 cm^{-1} for **1**[9] and 5 cm^{-1} for **2**.[11] The spectrum of **2** was measured more recently than that of **1** and the signal-to-noise ratio is significantly superior. The VCD spectra of **1** and **2** were scanned, digitized, and converted from ΔA to $\Delta\epsilon$ scales. In the case of **2**, the path length used was not reported. The value used here, 84 μm, was determined by comparison of the reported 5 cm^{-1} resolution absorption spectrum to a 5 cm^{-1} resolution spectrum of a 1.01 M CCl_4 solution of **2** using a 258 μm path cell measured using the Nicolet MX-1 FT spectrometer. The chemical and optical purities of the samples of **1** and **2** were not reported but were the highest available (L. A. Nafie, private communication). The C−H stretching VCD spectrum of **1** in CCl_4 solution was measured using a dispersive VCD spectrometer[3,5,24,25] at ∼10 cm^{-1} resolution. (1*R*,4*R*)-(+)-**1** and (1*S*,4*S*)-(−)-**1** were from Aldrich and had purities/specific rotations of 99%/$[\alpha]_D^{25} = +44.1°$ ($c = 10$, C_2H_5OH) and 99%/$[\alpha]_D^{20} = -43°$ ($c = 10$, C_2H_5OH), respectively. Enantiomeric purities are very close to 100%. The VCD spectrum of (1*R*,4*R*)-(+)-**1** was obtained

* Author to whom correspondence should be addressed.

⊗ Abstract published in *Advance ACS Abstracts,* August 1, 1997.

S1089-5639(97)01235-8 CCC: $14.00

as one half of the difference of the VCD spectra of (1*R*,4*R*)-(+)-**1** and (1*S*,4*S*)-(−)-**1**.

Absorption and VCD spectra of **1** and **2** were fit, using the equations[26,27]

$$\epsilon(\bar{\nu}) = \frac{8\pi^3 N}{3000hc(2.303)}\bar{\nu}\sum_i D_i f_i(\bar{\nu},\bar{\nu}_i) \quad (1)$$

$$\Delta\epsilon(\bar{\nu}) = \frac{32\pi^3 N}{3000hc(2.303)}\bar{\nu}\sum_i R_i f_i(\bar{\nu},\bar{\nu}_i) \quad (2)$$

where $\bar{\nu}_i$, D_i, and R_i are excitation frequencies, dipole strengths, and rotational strengths, respectively. The normalized bandshape, $f_i(\bar{\nu},\bar{\nu}_i)$, is assumed to be Lorentzian:

$$f_i(\bar{\nu},\bar{\nu}_i) = \frac{1}{\pi\gamma_i}\frac{\gamma_i}{[(\bar{\nu}-\bar{\nu}_i)^2+\gamma_i^2]} \quad (3)$$

where $\bar{\nu}_i$, is the half-width at half-height. Fitting was carried out using the PeakFit program (Jandel Scientific Software).

Ab initio calculations of the frequencies, dipole strengths, and rotational strengths of **1** and **2** were carried out within the harmonic approximation using the equations:[15−17]

$$D_i = |\langle 0|\vec{\mu}_{el}|1\rangle_i|^2 \quad (4)$$

$$R_i = \mathrm{Im}[|\langle 0|\vec{\mu}_{el}|1\rangle_i \cdot \langle 1|\vec{\mu}_{mag}|0\rangle_i] \quad (5)$$

$$\langle 0|(\mu_{el})_\beta|1\rangle_i = (\hbar/2\omega_i)^{1/2}\sum_{\lambda\alpha} S_{\lambda\alpha,i}P^{\lambda}_{\alpha\beta} \quad (6)$$

$$\langle 0|(\mu_{mag})_\beta|1\rangle_i = -(2\hbar^3\omega_i)^{1/2}\sum_{\lambda\alpha} S_{\lambda\alpha,i}M^{\lambda}_{\alpha\beta} \quad (7)$$

Here, $\hbar\omega_i = hc\bar{\nu}_i$ is the excitation energy of the *i*th fundamental, $P^{\lambda}_{\alpha\beta}$ and $M^{\lambda}_{\alpha\beta}$ are the atomic polar tensors (APTs) and atomic axial tensors (AATs), respectively, and the $S_{\lambda\alpha,i}$ matrix converts Cartesian displacement coordinates, $X_{\lambda\alpha}$, to normal coordinates, Q_i,

$$X_{\lambda\alpha} = \sum_i S_{\lambda\alpha,i}Q_i \quad (8)$$

$S_{\lambda\alpha,i}$ and ω_i are obtained simultaneously by diagonalization of the mass-weighted Cartesian harmonic force field (HFF) (the Hessian).

DFT HFFs, APTs, and AATs of **1** and **2** were calculated using direct, analytical derivative methods implemented within the GAUSSIAN program[28] as described previously.[1,2,15,29,30] In this work the hybrid functionals B3PW91 and B3LYP have been used. B3PW91 is the functional of Becke.[22] B3LYP is a subsequent functional[15,29] also incorporated in the GAUSSIAN program. All DFT calculations use the "fine" grid.[15,29]

HFFs, APTs, and AATs were also calculated at the Hartree−Fock/self-consistent field (HF/SCF) level of approximation, again using direct, analytical derivative methods and the GAUSSIAN program.[1]

Both DFT and HF/SCF AATs are calculated using GIAO basis sets. Accordingly, AATs are gauge-independent (common origin gauge and distributed origin gauge AATs[17,18] are identical) and common origin gauge AATs yield origin-independent rotational strengths.

Calculations use the 6-31G*[18,31] and TZ2P[18] basis sets. For **1** and **2** calculations using these [3s2p1d/2s] and [5s4p2d/3s2p] basis sets involve 197 and 463 basis functions, respectively.

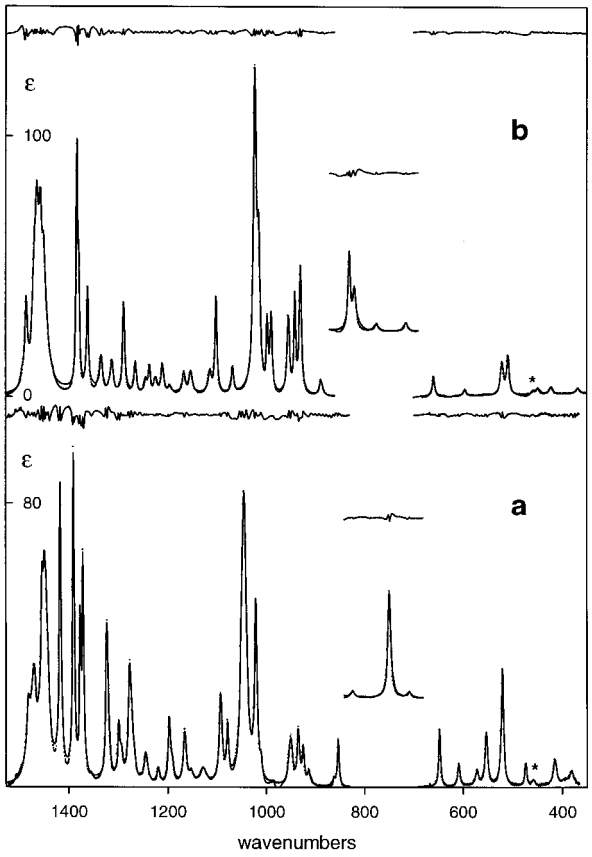

Figure 1. Absorption spectra of (1*R*,4*R*)-(+)-**1** (a) and (1*S*,4*S*)-(+)-**2** (b). Solid lines are 1 cm^{-1} resolution experimental spectra; dotted lines are Lorentzian fits. Difference spectra (spectrum minus fit) are also shown (solid lines above spectra). Spectra are for CCl_4 and CS_2 solutions: (a) 1525−830 cm^{-1} and 700−365 cm^{-1} in CCl_4 (0.45 M), 840−680 cm^{-1} in CS_2 (0.45 M); (b) 1525−860 cm^{-1} and 700−350 cm^{-1} in CCl_4 (1.01 M), 870−690 cm^{-1} in CS_2 (0.97 M). Asterisked bands are attributable to impurities.

Ab initio calculations were carried out using Silicon Graphics Power Challenge and IBM SP2 machines at USC and Lorentzian Inc.

Results

Mid-IR Spectral Region. The unpolarized absorption spectrum of an 0.45 M solution of **1** in CCl_4 over the range 1525−365 cm^{-1} is shown in Figure 1. In the region of strongest CCl_4 absorption, the spectrum of an 0.45 M solution of **1** in CS_2 is shown instead.

The frequencies and dipole strengths predicted for **1** using DFT, the B3PW91 functional, and the TZ2P basis set are given in Table 1. The absorption spectrum predicted thence, using Lorentzian band shapes with uniform width ($\gamma = 4$ cm^{-1}), over the range 350−1600 cm^{-1} is shown in Figure 2. Allowing for the expected small shift to higher frequency,[32] the calculated spectrum is in excellent overall qualitative agreement with the experimental spectrum, also shown in Figure 2. Assignment of a large majority of fundamentals 10−58 follows straightforwardly. With the exception of fundamentals 27 and 41, modes 10−50 are clearly identifiable in the experimental spectrum, as indicated in Figure 2. Mode 27 is predicted to be close to mode 26 and weak in intensity. Mode 41 is also predicted to be very weak. It is therefore not surprising that these modes are not readily apparent in the experimental spectrum. Modes 57 and 58 are also assignable. However, modes 51−56 are not well resolved and are not immediately assignable.

Quantitative analysis of the experimental absorption spectrum of **1**, guided by the above qualitative assignment, is carried out

TABLE 1: TZ2P Calculations for Camphor (1)[a]

	DFT								
	B3PW91			B3LYP			HF/SCF		
mode	ν	D	R	ν	D	R	ν	D	R
75	3131	26.3	−3.8	3122	29.2	−4.7	3267	45.1	−6.9
74	3119	20.8	3.6	3108	23.6	3.6	3252	20.4	10.9
73	3115	18.6	13.0	3102	65.1	20.6	3242	139.6	23.1
72	3113	59.2	−15.1	3098	16.2	−6.9	3238	20.6	−42.6
71	3111	7.8	23.8	3095	13.9	20.6	3236	1.6	30.2
70	3106	5.4	5.9	3093	6.4	−3.4	3230	20.2	27.3
69	3103	44.6	−4.4	3088	54.7	−7.4	3224	136.9	−22.1
68	3097	4.5	−0.4	3084	11.3	−23	3223	3.1	−25.4
67	3095	5.5	−20.3	3081	3.7	−0.7	3221	5.6	−3.1
66	3090	35.1	−4.5	3080	29.2	−2.9	3213	2.9	−0.8
65	3068	36.6	17.9	3062	34.9	21.5	3205	10.3	−10.3
64	3066	11.5	−3.5	3058	12.8	−4.4	3202	52.6	24.4
63	3059	27.1	−1.9	3054	27.4	−3.4	3191	33.4	1.8
62	3041	44.1	−7.9	3036	47.5	−6.8	3173	57.7	−18.4
61	3039	19.5	10.5	3033	19.4	10.9	3169	26.9	22.8
60	3036	18.9	−0.9	3030	15.9	−1.8	3164	16.0	−3.5
59	1821	553.5	18.0	1804	556.7	18.1	1996	659.1	16.5
58	1526	20.9	−1.3	1536	19.5	−1.0	1658	13.4	0.9
57	1512	18.2	13.1	1523	14.3	10.8	1645	8.8	6.7
56	1508	1.1	1.1	1518	1.8	1.3	1637	1.2	0.7
55	1496	15.2	0.0	1508	18.7	0.0	1627	10.4	1.1
54	1492	15.2	3.5	1503	9.4	1.9	1622	6.5	0.0
53	1485	19.3	6.2	1496	18.8	6.4	1615	19.8	2.6
52	1480	19.6	−2.2	1492	13.8	−1.1	1612	10.3	−0.2
51	1477	9.0	−1.2	1489	11.2	−1.5	1609	11.0	−1.1
50	1450	39.5	−4.8	1464	36.2	−4.3	1595	24.1	−4.8
49	1419	38.0	−8.7	1432	31.4	−7.1	1557	18.7	−4.3
48	1404	20.5	3.7	1416	19.5	2.8	1544	9.7	2.2
47	1398	26.0	−1.0	1410	19.7	−0.3	1538	12.5	−1.0
46	1349	20.1	10.5	1345	12.0	6.3	1475	16.5	13.0
45	1330	5.1	−6.4	1335	3.3	−1.9	1460	1.7	0.2
44	1325	5.3	−5.9	1326	8.1	−3.2	1450	3.4	−9.5
43	1302	30.8	−1.0	1299	26.3	−2.9	1434	21.5	−2.0
42	1274	9.5	26.8	1274	7.8	19.0	1395	6.1	20.5
41	1266	0.4	3.9	1265	0.2	3.1	1393	5.8	4.1
40	1247	6.3	1.6	1246	9.4	3.6	1361	5.6	−1.2
39	1222	14.5	−4.2	1225	15.7	−5.7	1330	12.5	−7.8
38	1216	2.2	−3.1	1214	3.1	2.6	1327	1.2	3.5
37	1188	11.4	17.9	1189	12.7	18.3	1291	8.7	7.5
36	1171	2.3	−6.4	1167	1.3	−5.6	1282	8.0	3.9
35	1147	4.4	8.5	1144	5.6	7.9	1245	5.9	2.3
34	1113	19.5	−4.2	1118	16.3	−3.6	1218	15.7	−2.9
33	1097	7.8	−0.3	1102	5.7	−3.8	1195	7.6	−3.1
32	1059	119.6	−38.7	1055	61.9	−30.0	1156	69.6	−41.8
31	1038	47.2	−13.5	1037	100.1	−0.8	1129	50.6	−11.0
30	1029	3.4	7.4	1030	11.4	−14.0	1115	3.4	5.1
29	1003	1.5	−3.4	998	0.2	0.4	1075	0.4	0.9
28	967	13.4	−10.5	961	8.9	9.8	1038	10.1	1.3
27	956	2.8	−3.1	957	7.5	−22.1	1030	1.7	−13.9
26	951	10.9	12.8	943	3.3	14.7	1023	8.7	29.1
25	939	7.4	24.2	939	14.2	18.1	1014	7.0	−0.8
24	925	4.4	−11.4	920	4.9	−7.6	994	1.3	−5.1
23	877	4.6	−11.0	868	4.6	−14.4	937	1.5	0.9
22	863	7.2	−15.3	855	7.8	−16.4	925	10.5	−14.3
21	837	2.0	−1.5	836	2.3	−1.2	898	1.3	1.6
20	757	45.7	30.0	751	42.9	32.3	819	19.0	18.0
19	713	3.7	−10.2	708	2.9	−8.2	771	1.3	−2.5
18	652	11.8	−8.3	645	14.2	−12.9	689	17.1	−21.8
17	614	6.7	−30.0	616	5.8	−24.9	671	5.6	−4.6
16	574	6.2	6.4	572	5.9	6.1	614	4.5	2.1
15	557	16.2	−16.4	558	15.9	−13.7	597	15.7	−10.9
14	522	35.6	8.0	523	33.2	7.1	563	48.3	8.4
13	475	4.9	2.6	475	4.8	2.3	508	9.1	1.8
12	413	11.5	2.1	417	11.7	1.9	447	14.8	1.8
11	388	1.6	1.6	393	1.9	1.7	421	2.4	2.2
10	379	8.1	1.9	381	7.9	1.1	412	11.6	−0.2
9	294	26.3	−3.3	298	21.7	1.1	321	25.4	4.0
8	293	0.9	−1.9	293	6.6	−6.5	313	15.1	−9.3
7	259	13.6	1.4	262	12.0	1.4	280	11.0	2.4
6	236	10.1	1.5	239	11.6	1.3	259	10.5	−1.8
5	222	8.8	−0.6	223	7.5	−1.0	247	11.0	−1.2
4	211	3.5	−3.2	213	3.0	−2.4	239	2.2	0.9
3	172	1.5	−3.5	178	1.2	−3.2	210	3.3	−0.6
2	166	1.4	2.4	167	1.7	3.2	178	6.0	5.8
1	109	140.5	−3.7	110	142.8	−3.7	117	164.8	−5.8

[a] ν in cm^{-1}, D in 10^{-40} esu^2 cm^2, R in 10^{-44} esu^2 cm^2. Rotational strengths are for the (1*R*,4*R*) enantiomer.

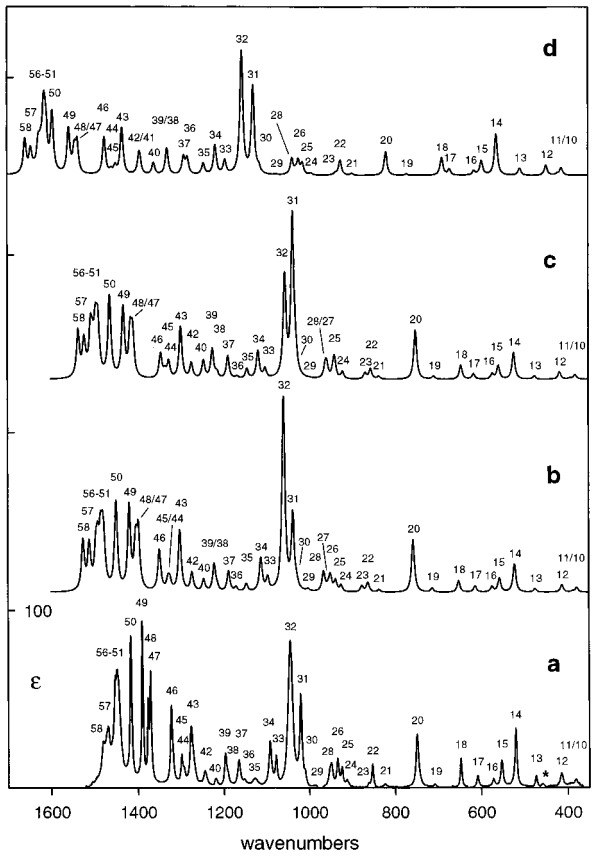

Figure 2. Experimental (a) and calculated (b−d) absorption spectra of **1**. The experimental spectrum is from Figure 1a (1525−840 and 680−365 cm^{-1} in CCl_4; 840−680 cm^{-1} in CS_2). Calculated spectra are (b) DFT/B3PW91/TZ2P; (c) DFT/B3LYP/TZ2P; (d) HF/SCF/TZ2P. $\gamma = 4$ cm^{-1} for all bands in (b−d). The asterisked band in (a) is not due to **1**. Numbers indicate fundamentals.

by Lorentzian fitting. The fits are shown in Figure 1. Their accuracies are documented by the difference spectra (experimental spectrum − fit), also shown in Figure 1. The frequencies, dipole strengths, and bandwidths obtained are listed in Table 2, together with their assignments. Below 900 cm^{-1} we have found no evidence of bands other than fundamentals 10−23. In the range 900−975 cm^{-1}, in addition to fundamentals 24, 25, 26, and 28 a band is clearly present on the higher energy side of band 28. This could be a fundamental, in which case the B3PW91/TZ2P calculation incorrectly orders modes 27 and 28; alternatively, it could be a nonfundamental, mode 27 remaining undetected. In the range 975−1425 cm^{-1} , the fundamentals 29−50 are all present and, in addition, three weak bands assignable as nonfundamentals are also identified. The absorption at 1240−1250 cm^{-1} is fit with two unresolved bands separated by ∼4 cm^{-1}; the lower frequency, weaker band is assigned as fundamental 41. The absorption above 1425 cm^{-1} is fit with nine bands, one greater than the number of fundamentals predicted in this region. The assignment of modes 57 and 58 is well-defined. The band in between these two modes is assigned as a nonfundamental. The bands in the region 1425−1465 cm^{-1} are assigned to modes 51−56. In this region the fit is obviously not unique.

The frequencies and dipole strengths predicted for **1** using the B3LYP functional and the TZ2P basis set are also given in Table 1. The absorption spectrum predicted thence over the range 350−1600 cm^{-1} is also shown in Figure 2. The spectra predicted using the B3PW91 and B3LYP functionals are qualitatively identical, with the exception of modes 24−28 and 31−32. Using B3LYP, mode 26 is very weak and modes 27 and 28 are unresolved. The resulting triplet structure is in poorer

TABLE 2: Experimental Parameters for Camphor (1)[a]

	absorption			VCD[d]		
mode[b,c]	ν	D	γ	ν	R[e]	γ
58	1481	17.9	5.2	1479	−4.9	4.6
	1475	5.7	4.6	1475	6.8	5.7
57	1469	22.9	5.1	1471	16.2	6.1
56	1462	1.4	5.0	1464	−1.3	2.4
55	1455	14.6	5.9	1458	1.5	5.6
54	1453	15.3	3.0	1452	4.1	6.1
53	1448	30.1	4.5	1451	5.5	7.1
52	1445	21.7	4.5	1447	−2.6	1.8
51	1439	7.3	4.5	1443	−2.3	2.2
50	1417	40.2	2.4	1418	−6.8	2.8
49	1390	38.5	2.0	1391	−8.8	3.1
48	1377	17.0	2.0	1378	4.3	3.3
47	1371	26.5	2.1	1373	−2.8	3.1
	1354	1.3	3.6			
46	1323	29.8	3.0	1323	11.4	3.1
45	1299	10.9	3.2	1299	−19.0	4.4
44	1293	3.5	3.1	1294	2.3	6.1
43	1277	26.9	3.7	1281	4.3	6.4
	1271	7.4	4.2			
42	1245	8.3	4.5	1247	35.2	5.6
41	241	1.0	6.1	1240	−6.0	6.1
40	1220	3.4	3.3	1220	−3.4	5.6
39	1197	12.9	2.9	1201	−6.5	3.3
38	1191	3.4	2.9	1195	−2.6	3.1
37	1166	12.5	3.4	1169	19.8	4.0
36	1153	4.0	5.2	1155	−11.2	5.4
35	1128	8.6	7.6	1132	10.6	9.1
34	1093	22.4	3.4	1099	−4.2	3.3
33	1079	9.4	2.3			
	1051	8.2	2.7			
32	1045	123.6	5.6	1047	−72.2	5.6
				1036	5.6	2.2
31	1021	40.2	2.9	1022	−19.3	4.9
30	1011	2.7	2.5	1011	8.2	2.8
29	986	0.5	3.0	982	−15.2	9.4
	955	4.0	2.9	958	7.9	3.8
28	950	12.1	3.1	950	−28.5	3.9
27						
26	935	15.2	3.2	934	14.7	3.4
25	925	8.0	2.7	926	28.8	2.8
24	913	4.3	3.3	914	−27.5	3.5
23	862	2.6	3.7			
22	853	8.7	2.0			
21	824	2.9	4.5			
20	749	40.2	3.4			
19	709	3.1	5.0			
18	648	15.6	2.2			
17	609	9.1	2.9			
16	572	8.7	4.0			
15	553	25.6	3.3			
14	521	51.0	2.8			
13	474	9.6	2.5			
12	415	22.8	4.4			
11	396	6.6	7.3			
10	381	20.3	6.8			

[a] From Lorentzian fitting to experimental absorption and VCD spectra in CCl_4 solution (Figures 1 and 3); ν and γ in cm^{-1}, D in 10^{-40} esu^2 cm^2, R in 10^{-44} esu^2 cm^2. [b] Assignment. [c] Modes 21−19 were measured in CS_2 solution. [d] For the (1*R*,4*R*)-(+) enantiomer. [e] Rotational strengths are not normalized to 100% ee.

TABLE 3: 6-31G* Calculations for Camphor (1)[a]

	DFT								
	B3PW91			B3LYP			HF/SCF		
mode	ν	D	R	ν	D	R	ν	D	R
59	1857	463.3	18.9	1841	454.3	18.2	2038	579.6	18.2
58	1554	14.0	−1.9	1559	10.8	−1.0	1681	9.1	0.4
57	1541	16.1	11.5	1547	11.3	7.9	1668	8.1	5.7
56	1536	1.0	1.6	1541	0.8	1.3	1659	1.0	1.0
55	1524	9.4	0.4	1531	9.0	0.5	1651	5.9	0.5
54	1520	10.9	5	1526	6.6	3.1	1645	5.3	−0.3
53	1514	14.6	3.1	1520	12.2	2.5	1639	11.5	1.6
52	1509	19.1	−1.2	1516	13.0	0.1	1637	10.9	−0.2
51	1505	7.0	0.4	1512	6.5	0.8	1633	7.1	0.5
50	1480	29.7	−3	1488	24.8	−2.1	1619	19.0	−3.3
49	1447	29.2	−7.2	1455	18.9	−5.2	1582	13.6	−3.5
48	1430	15.7	3.5	1437	11.8	2.6	1568	6.4	2.0
47	1426	19.9	−1.8	1434	12.3	−1.1	1563	9.5	−1.2
46	1366	20.3	9.9	1361	14.2	7.3	1492	17.8	10.6
45	1344	4.6	−5.2	1347	2.4	−3.8	1475	1.2	0.3
44	1340	4.7	−6.9	1339	6.7	−3.3	1462	5.3	−8.3
43	1316	26.6	−2.1	1312	21.6	−3.4	1449	21.4	−3.4
42	1287	10.7	27.4	1284	10.0	19.6	1411	0.7	−1.1
41	1280	1.0	1.8	1279	0.1	1.4	1406	14.5	26.9
40	1260	7.0	1.5	1258	10.6	1.9	1375	5.6	−1.6
39	1234	16.1	−6.1	1235	17.5	−8.4	1341	9.0	−8.6
38	1229	2.0	−2.1	1225	2.7	3.1	1339	4.2	4.7
37	1199	10.9	16.9	1197	12.5	17.6	1302	5.0	1.7
36	1185	3.3	−7.3	1181	2.0	−6.7	1294	11.0	7.1
35	1159	3.6	7.8	1155	3.9	7.4	1258	3.2	0.6
34	1124	20.2	−5.9	1128	17.7	−4.6	1227	16.0	−1.5
33	1106	7.2	−0.6	1108	5.5	−4.8	1205	7.5	−1.9
32	1070	127.8	−35.8	1064	77.0	−27.6	1168	79.9	−42.3
31	1048	47.7	−14.4	1045	97.2	−0.5	1139	45.5	−8.4
30	1040	5.4	9.0	1040	7.8	−11	1125	3.0	5.9
29	1015	1.3	−3.3	1009	0.3	−0.6	1087	0.4	0.2
28	978	13.3	−10.2	970	11.5	4.7	1048	8.8	−0.3
27	967	2.4	−4.6	966	4.2	−17.8	1040	1.6	−12.5
26	961	9.7	11.0	950	1.5	0.8	1033	8.9	27.0
25	949	7.5	23.9	949	13.0	27.6	1023	5.6	0.6
24	932	4.6	−14.6	926	5.6	−11.2	1002	1.8	−7.3
23	884	3.9	−7.3	875	3.2	−8.9	945	2.1	4.7
22	869	6.3	−10.6	861	6.2	−10.3	933	10.6	−13.7
21	845	2.2	−0.1	842	2.5	−0.2	906	1.3	2.2
20	765	36.9	22.9	758	34.2	23.7	827	13.7	12.8
19	718	3.2	−8.6	712	2.5	−6.9	776	1.3	−0.7
18	654	9.4	−6.9	647	11.0	−10.0	693	15.8	−17.2
17	616	6.8	−28.5	616	6.0	−23.8	673	5.8	−7.7
16	575	6.2	5.9	572	6.0	6.2	615	4.7	2.5
15	556	14.6	−14.0	556	14.2	−12.5	598	15.2	−10.3
14	523	36.7	8.5	522	34.7	7.2	563	49.1	8.4
13	476	4.4	2.3	475	4.5	2.1	509	9.2	1.6
12	417	11.5	1.5	417	11.9	1.3	449	15.7	1.3
11	393	1.4	1.0	396	1.4	1.0	424	1.7	1.8
10	382	8.5	1.8	382	8.2	1.1	413	13.2	−1.0
9	297	2.6	−4.8	299	21.7	0.3	322	24.3	3.3
8	296	24.5	−0.4	295	7.3	−5.4	315	18.2	−8.8
7	262	14.3	1.6	262	13.6	1.6	280	13.0	3.0
6	238	9.3	1.2	238	13.0	1.8	258	12.2	−1.0
5	226	12.4	−0.3	222	7.9	−1.2	246	10.8	−0.9
4	209	3.2	−2.8	208	2.5	−2.2	237	2.1	−0.3
3	168	1.6	−1.0	166	3.0	−6.1	208	2.2	−0.9
2	163	3.6	−3.3	162	1.8	2.7	180	5.4	5.8
1	107	133.6	−2.2	107	134.7	−1.9	117	165.0	−4.4

[a] Units as in Table 1.

agreement with the experimental spectrum. The relative intensities of modes 31 and 32 are inverted and, again, in worse agreement with experiment. The accuracy of the B3LYP functional thus appears to be lower than that of the B3PW91 functional.

The VCD spectrum of an 0.60 M solution of **1** in CCl_4 over the range 1500−900 cm^{-1} at a resolution of 4 cm^{-1}, reported by Nafie,[9] is shown in Figure 3. Strong VCD is observed at the frequencies of the absorption bands assigned above to fundamentals 24, 25, 28, 30, 31, 32, 36, 37, 42, 46−50, and 57. In addition, the pairs of modes 38/39 and 44/45 and the set 51−54 give rise to strong, but unresolved, VCD. Weaker VCD is observed corresponding to the modes 34, 35, and 43. VCD attributable to modes 26, 27, 29, 33, 40, 41, 55, 56, and 58 is not clearly visible.

Quantitative analysis of the VCD spectrum of **1** is carried out using Lorentzian fitting as shown in Figure 3. The accuracy of the fit is shown by the difference spectrum. In contrast to the difference spectrum resulting from fitting the absorption spectrum, where the variations reflect primarily the quality of the fitting and experimental noise is relatively insignificant, the VCD difference spectrum is dominated by experimental noise, being relatively uniform except in the region of the intense

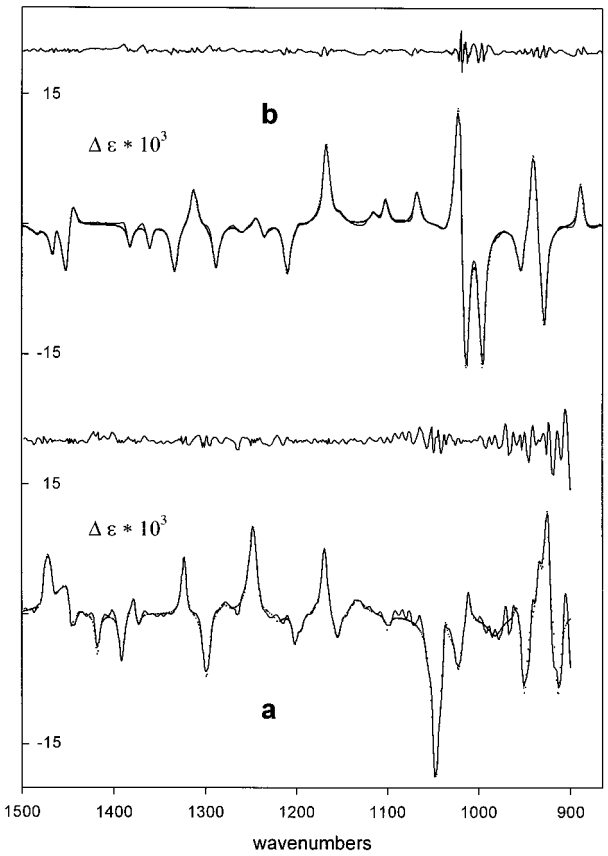

Figure 3. VCD spectra of (1*R*,4*R*)-(+)-**1** (a) and (1*S*,4*S*)-(+)-**2** (b). Solid lines are experimental spectra; dotted lines are Lorentzian fits. Difference spectra (spectrum minus fit) are also shown (solid lines above spectra). The spectra are of 0.6 M (a) and 1.0 M (b) solutions in CCl_4 from ref 7 (a) and ref 9 (b). Data above 1500 cm^{-1} have been deleted.

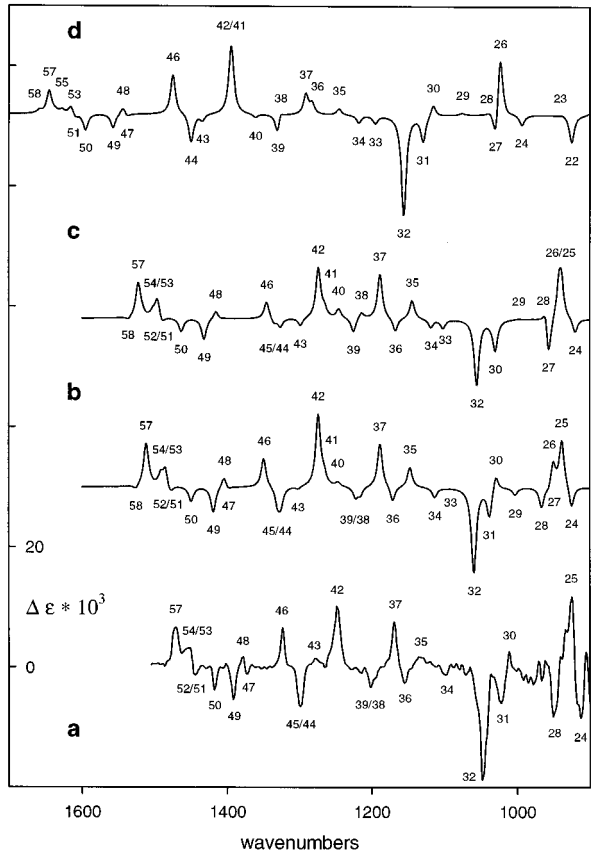

Figure 4. Experimental (a) and calculated (b−d) VCD spectra of **1**. The experimental spectrum is from Figure 3a. Calculated spectra are (b) DFT/B3PW91/TZ2P; (c) DFT/B3LYP/TZ2P; (d) HF/SCF/TZ2P. $\gamma = 4$ cm^{-1} for all bands in (b−d). Numbers indicate fundamentals.

absorption at ∼1050 cm^{-1} and below 1000 cm^{-1} where instrumental sensitivity deteriorates significantly. The frequencies, rotational strengths and bandwidths resulting are given in Table 2. It should be noted that due to the different spectrometers and resolutions used in obtaining the absorption and VCD spectra, it is not possible to constrain either frequencies or bandwidths to be identical in the VCD and absorption spectra. As seen in Table 2, the frequency differences for corresponding bands are small and the bandwidths are generally greater for the VCD spectrum, as expected given its lower resolution.

The VCD in the range 900−975 cm^{-1} is fit with five bands, corresponding to the five absorption bands in this region. In addition to the clearly visible bands due to modes 24, 25, and 28, bands with positive VCD are found corresponding to mode 26 and to the absorption band to higher energy of mode 28. A broad, weak, negative band, attributable to mode 29, is found in the range 975−1000 cm^{-1}; considerable uncertainty attaches to its rotational strength due to the high noise level in this region. In addition to modes 30, 31, and 32, weak positive VCD is found between modes 31 and 32. Modes 38 and 39 are not clearly resolved in the VCD spectrum; fitting yields two negative bands, the VCD of mode 39 being the greater. Between modes 39 and 42, two bands attributable to modes 40 and 41 are found; both exhibit weak and negative VCD. Modes 44 and 45 are not clearly resolved in the VCD spectrum; fitting yields two bands of opposite sign and very different intensities: the VCD of mode 44 is weak and positive, while that of mode 45 is strong and negative. As for the absorption spectrum, the complex region above 1425 cm^{-1} is fit using nine bands. With the exception of mode 57, whose VCD is clearly resolved, the rotational strengths of these bands are substantially uncertain as a result of their lack of resolution and/or the weakness of their VCD.

The rotational strengths predicted for **1** using B3PW91 and TZ2P are given in Table 1. The VCD spectrum predicted thence assuming Lorentzian bands of constant width ($\gamma = 4.0$ cm^{-1}) is shown in Figure 4, together with the experimental spectrum. Overall, the qualitative agreement of the predicted and experimental VCD spectra is excellent. The predicted VCD of modes 24−26, 28−39, 42, and 46−50 is in perfect qualitative agreement with the results of Lorentzian fitting to the experimental spectrum with regard to both sign and intensity. The VCD of mode 27 is predicted to be weak; it is therefore not surprising that it is not detected. The VCD of modes 40 and 41 are predicted to be weak and positive, consistent with experiment with regard to magnitude, but not sign. The VCD of mode 43 is predicted to be weak, as observed, but negative in sign, opposite to experiment. The VCD of modes 44 and 45 are predicted to be of the same, negative sign and similar in magnitude; fitting yields two bands of opposite sign and very different magnitude. The VCD predicted for the set of modes 51−58 is in good overall qualitative agreement with experiment.

The rotational strengths predicted using B3LYP and TZ2P are also given in Table 1. The VCD spectrum predicted thence is also shown in Figure 4. As for the absorption spectrum, B3PW91 and B3LYP give significantly different predictions for modes 24−28 and 30−32. Again, B3PW91 gives results in clearly superior agreement with experiment. Qualitative differences are also found for modes 29, 33, 38, and 44/45. In each case, the B3PW91 prediction is superior.

The B3PW91/TZ2P calculations result in essentially unambiguous assignment of all fundamentals 10−58, with the exception of 27 and 51−56. Mode 27 is not detected in either

TABLE 4: TZ2P Calculations for Fenchone (2)[a]

	DFT								
	B3PW91			B3LYP			HF/SCF		
mode	ν	D	R	ν	D	R	ν	D	R
59	1815	440.4	−7.3	1797	443.3	−7.4	1989	540.9	−5.3
58	1524	23.4	−7.6	1535	20.0	−5.7	1662	14.7	−1.8
57	1508	31.9	−6.8	1518	27.3	−6.2	1641	19.3	−2.3
56	1500	31.6	6.6	1511	32.1	6.6	1636	16.3	0.7
55	1496	5.0	−0.1	1507	3.5	−4.6	1625	12.7	−3.8
54	1493	23.3	−17.1	1504	21.3	−13.1	1624	6.2	−6.4
53	1489	23.3	3.0	1499	16.3	3.5	1615	11.7	−0.9
52	1483	8.5	−2.3	1493	10.7	−7.0	1613	6.9	1.9
51	1479	6.4	1.6	1492	5.4	5.5	1610	11.0	−0.5
50	1475	3.5	1.1	1487	4.8	1.6	1606	3.4	0.4
49	1410	21.6	−7.2	1422	30.6	−1.3	1549	18.3	−2.0
48	1409	31.0	2.5	1420	13.2	−1.4	1545	6.9	−0.1
47	1386	18.8	−4.0	1399	14.6	−2.1	1527	8.3	−2.4
46	1360	4.5	−11.9	1357	4.4	−12.7	1489	11.1	−10.1
45	1342	7.8	11.5	1344	5.8	9.9	1475	9.1	8.1
44	1315	16.1	−9.2	1318	15.7	−8.8	1451	8.6	−4.9
43	1292	8.4	−1.0	1291	7.6	−1.2	1419	4.7	−1.3
42	1272	1.6	1.9	1275	3.6	5.0	1395	3.9	5.7
41	1263	4.8	1.2	1266	1.6	−1.6	1386	3.1	−2.5
40	1247	8.1	−0.4	1244	9.0	−2.4	1369	4.2	0.6
39	1236	9.1	−13.3	1235	9.4	−12.3	1345	13.9	−16.4
38	1218	1.3	0.8	1216	1.2	−0.9	1326	0.7	−3.6
37	1189	7.5	23.5	1188	10.0	24.8	1300	6.8	20.4
36	1176	7.6	3.6	1174	7.4	4.5	1288	7.7	3.5
35	1134	7.7	5.3	1130	7.0	3.7	1232	10.7	−4.3
34	1122	19.4	10.3	1125	17.0	3.8	1224	14.2	9.6
33	1086	5.7	5.9	1090	6.2	4.2	1185	6.8	12.2
32	1037	71.9	73.8	1040	39.5	67.4	1133	84.7	58.2
31	1029	96.1	−59.6	1028	81.9	−49.4	1120	31.0	−57.0
30	1011	18.8	−36.8	1015	20.9	−26.8	1100	11.9	−15.9
29	1002	20.7	−0.5	1004	54.0	−6.5	1090	30.2	−5.4
28	968	17.4	−2.9	962	15.0	−8.9	1040	20.6	−8.9
27	959	0.6	1.1	959	3.0	−1.0	1034	1.9	−2.4
26	955	32.1	19.2	949	36.5	23.1	1023	18.4	18.1
25	938	45.8	−29.0	929	51.1	−25.4	1011	24.2	−17.3
24	901	3.1	14.1	892	4.1	13.1	961	1.5	9.7
23	899	1.8	−0.8	887	1.7	0.5	949	1.7	0.1
22	845	6.3	−6.2	843	2.9	−4.3	914	2.1	−5.2
21	841	16.4	6.6	832	16.9	24.3	901	20.2	4.8
20	829	17.7	−0.6	827	19.2	−21.8	893	20.7	7.4
19	787	2.1	2.8	785	2.0	3.0	849	3.7	0.9
18	723	3.9	1.5	718	4.0	2.1	781	4.5	−2.4
17	661	13.1	6.4	657	11.9	5.9	709	1.5	3.0
16	598	4.0	−0.8	595	3.6	−0.9	637	1.6	0.2
15	521	18.3	6.4	521	17.2	6.3	561	28.7	7.3
14	508	16.5	−2.7	510	17.8	−2.1	545	24.6	−2.0
13	436	6.0	6.7	443	5.6	5.9	479	4.6	4.3
12	418	4.9	−6.0	421	5.5	−5.2	452	8.3	−5.6
11	368	3.6	3.4	371	3.5	3.2	396	3.2	3.1
10	322	1.7	5.5	325	1.6	5.1	349	1.8	4.1
9	297	6.4	−0.6	299	10.7	−0.4	322	12.6	−0.6
8	289	72.4	−2.2	293	67.3	−1.8	316	84.4	−2.2
7	256	6.5	−0.4	259	4.9	−0.4	280	3.9	−0.9
6	231	12.3	−2.9	234	11.5	−1.9	251	8.5	−0.4
5	209	15.5	1.5	213	14.4	0.5	232	15.4	−0.6
4	194	16.5	7.6	196	15.7	7.7	219	11.7	3.6
3	188	1.3	0.2	191	1.0	−0.9	214	4.7	−3.6
2	179	19.6	0.7	183	20.6	0.8	201	30.4	3.7
1	82	111.3	0.7	85	112.1	0.5	94	128.0	0.0

[a] ν in cm^{-1}, D in 10^{-40} esu^2 cm^2, R in 10^{-44} esu^2 cm^2. Rotational strengths are for the (1*S*,4*S*) enantiomer.

absorption or VCD spectra. Modes 51−56 are unresolved and their detailed assignment is clearly not unambiguous.

The unpolarized spectrum of a 1.01 M solution of **2** in CCl_4 over the range 1525−350 cm^{-1} is shown in Figure 1. In the region of strongest CCl_4 absorption the spectrum of an 0.97 M solution of **2** in CS_2 is shown instead.

The frequencies and dipole strengths predicted for **2** using B3PW91 and TZ2P are given in Table 4. The absorption spectrum predicted thence over the range 350−1600 cm^{-1} is shown in Figure 5. Overall, it is in excellent qualitative agreement with the experimental spectrum, also shown in Figure

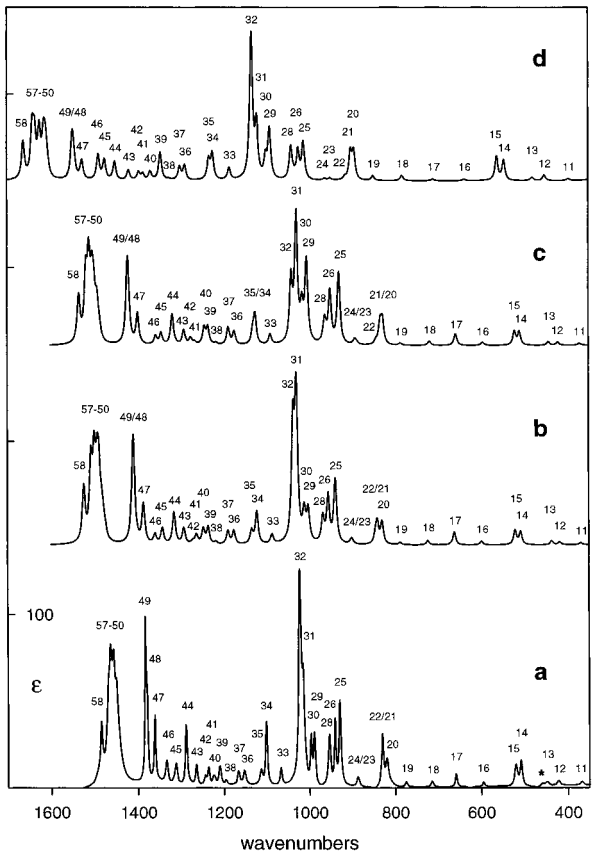

Figure 5. Experimental (a) and calculated (b−d) absorption spectra of **2**. The experimental spectrum is from Figure 1b (1525−860 and 690−350 cm^{-1} in CCl_4; 860−690 cm^{-1} in CS_2). Calculated spectra are (b) DFT/B3PW91/TZ2P; (c) DFT/B3LYP/TZ2P; (d) HF/SCF/TZ2P. $\gamma = 4$ cm^{-1} for all bands in (b−d). The asterisked band in (a) is not due to **2**. Numbers indicate fundamentals.

5. With the exception of fundamentals 21−24, 27, and 50−57, the fundamentals 11−58 are clearly resolved in the experimental spectrum, as indicated in Figure 5. The two pairs of modes 21/22 and 23/24 are not resolved, consistent with predicted splittings of 4 and 2 cm^{-1}. Mode 27 is predicted to be very weak and is not visible. Modes 50−57 are predicted within a span of 33 cm^{-1} and, not surprisingly, are not individually resolved experimentally.

A Lorentzian fit to the experimental absorption spectrum of **2** is shown in Figure 1. The corresponding parameters are given in Table 5, together with the band assignments. All bands are assigned as fundamentals. Of the fundamentals 11−58, only modes 22, 27, and 55 are missing. Above 1400 cm^{-1}, the absorption is fit with eight bands. The fit is not unique. Only in the case of mode 58 is the assignment well-defined.

The frequencies and dipole strengths predicted for **2** using B3LYP and TZ2P are also given in Table 4. The absorption spectrum predicted thence over the range 350−1600 cm^{-1} is also shown in Figure 5. The spectra predicted using the B3PW91 and B3LYP functionals are overall qualitatively very similar. The largest difference is for modes 29−32. The B3PW91 calculation is in better agreement with experiment, but in neither case are the relative intensities of modes 31 and 32 correctly predicted.

The VCD spectrum of a 1.0 M solution of **2** in CCl_4 over the range 865−1500 cm^{-1} at a resolution of 5 cm^{-1} , reported by Nafie,[11] is shown in Figure 3. Strong VCD is observed at the frequencies of the absorption bands assigned above to fundamentals 25, 26, 28, 30−34, 37, 39, and 44−46. Weaker VCD is observed corresponding to the modes 35, 36, 38, 41−43, 47−49, and 58. The unresolved modes 23/24 and 50−57

TABLE 5: Experimental Parameters for Fenchone (2)[a]

	absorption			VCD[d]		
mode[b,c]	ν	D	γ	ν	R^e	γ
58	1485	23.5	3.9	1484	−3.1	7.0
57	1469	24.4	4.2	1466	−11.4	4.4
56	1464	47.1	4.4	1463	7.0	4.2
55						
54	1457	43.4	4.3	1453	−12.6	4.8
53	1450	21.5	3.6	1451	5.2	5.0
52	1446	15.0	5.2	1451	−4.8	2.7
51	1440	6.0	6.5	1445	5.4	4.5
50	1432	5.5	6.5	1443	1.1	3.5
49	1383	36.6	1.9	1382	−6.9	3.6
48	1379	14.2	1.7	1381	2.1	2.8
47	1362	20.5	2.4	1361	−4.1	3.0
46	1335	14.0	4.7	1334	−13.5	4.5
45	1313	11.1	4.0	1313	11.0	4.6
44	1289	20.9	2.6	1288	−12.7	4.5
43	1265	8.9	3.2	1259	−2.7	5.5
42	1245	4.5	3.6	1244	2.7	4.4
41	1237	5.9	2.5	1235	−3.0	3.6
40	1224	5.9	4.2	1221	0.3	2.6
39	1210	9.2	3.3	1210	−14.4	4.2
38	1195	4.2	5.6	1197	0.4	2.5
37	1167	7.5	3.6	1167	25.9	4.5
36	1153	10.5	4.8	1152	2.0	4.5
35	1114	9.9	4.6	1115	3.7	5.0
34	1102	24.4	2.5	1102	6.2	3.5
33	1068	9.0	3.3	1067	10.2	4.0
				1035	−8.1	7.3
32	1023	114.3	3.4	1021	74.6	5.2
31	1015	49.9	3.5	1014	−73.6	4.6
30	997	14.8	2.0	996	−42.0	3.7
29	989	21.0	2.5	989	−2.8	3.7
28	954	26.8	3.0	954	−21.7	5.1
27						
26	941	22.2	2.0	940	30.9	4.0
25	930	42.2	2.8	929	−38.0	4.0
24	888	5.1	3.2	889	12.0	3.0
23	885	3.1	6.3	879	−2.2	6.4
22						
21	830	29.4	3.0			
20	820	20.4	3.8			
19	775	5.5	5.4			
18	715	6.5	4.8			
17	659	10.8	3.2			
16	596	4.2	3.4			
15	521	23.8	3.5			
14	509	23.6	2.9			
13	449	4.7	3.3			
12	422	6.5	3.6			
11	368	5.2	3.3			

[a] From Lorentzian fitting to experimental absorption and VCD spectra in CCl_4 solution (Figures 1 and 3); ν and γ in cm^{-1}, D in 10^{-40} esu^2 cm^2, R in 10^{-44} esu^2 cm^2. [b] Assignment. [c] Modes 21−18 were measured in CS_2 solution. [d] For the (1*S*,4*S*)-(+) enantiomer. [e] Rotational strengths are not normalized to 100% ee.

give rise to strong, but unresolved, VCD. VCD attributable to modes 27, 29, and 40 is not clearly visible.

A Lorentzian fit of the experimental VCD spectrum is shown in Figure 3. The VCD spectrum of **2** is less noisy than the VCD spectrum of **1** and this is clearly reflected in the difference spectrum for **2**. The frequencies, rotational strengths, and bandwidths obtained are given in Table 5. In addition to the fundamentals identified above, weak negative VCD attributable to fundamental 29 is found as a shoulder on the strong negative VCD of mode 30; weak positive VCD attributable to fundamental 40 is found between the negative VCD of modes 39 and 41; and VCD not assignable to fundamentals is found at 1035 cm^{-1}. The VCD of modes 50−57 is not fully resolved, and the fit is obviously not unique.

The rotational strengths predicted for **2** using B3PW91 and TZ2P are given in Table 4. The VCD spectrum predicted thence

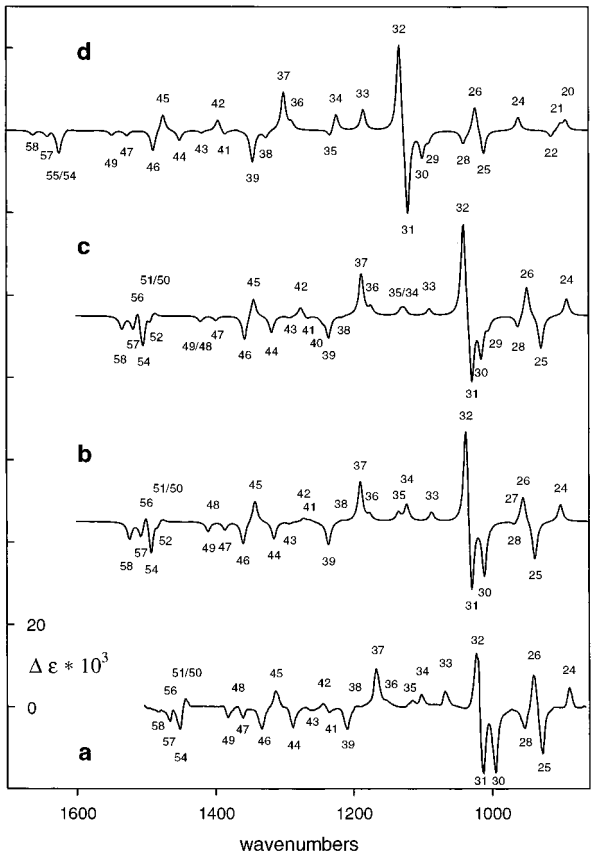

Figure 6. Experimental (a) and calculated (b−d) VCD spectra of **2**. The experimental spectrum is from Figure 3b. Calculated spectra are (b) DFT/B3PW91/TZ2P; (c) DFT/B3LYP/TZ2P; (d) HF/SCF/TZ2P. $\gamma = 4$ cm^{-1} for all bands in (b−d). Numbers indicate fundamentals.

is shown in Figure 6. Overall, the qualitative agreement of the predicted and experimental VCD spectra is excellent. The predicted VCD of modes 23−26, 28−39, 42−49, and 58 is in perfect qualitative agreement with the results of Lorentzian fitting with regard to both sign and intensity. The VCD of mode 27 is predicted to be weak and it is not surprising that it is not detected. The VCD of modes 40 and 41 are predicted to be weak with negative and positive signs respectively, consistent with experiment with regard to magnitude but not sign. The VCD predicted for modes 50−57 is in good overall qualitative agreement with experiment.

The rotational strengths predicted using B3LYP and TZ2P are also given in Table 4. The VCD spectrum predicted thence is also shown in Figure 6. As for the absorption spectra, B3PW91 and B3LYP predict very similar VCD spectra. For modes 29−32, the B3PW91 calculation is again in slightly better agreement with experiment.

The B3PW91/TZ2P calculations result in essentially unambiguous assignment of all fundamentals 10−58 with the exception of 27 and 50−57. Mode 27 is not detected in either absorption or VCD spectra. Modes 50−57 are unresolved and their detailed assignment is not unambiguous.

C═O Stretching Spectral Region. **1** and **2** exhibit very strong absorption at 1745 and 1742 cm^{-1} (in CCl_4 solution), respectively, attributable to the C═O stretching modes (59). Weak VCD in the C═O stretch of **1** was reported by Stephens and Clark.[5] The anisotropy ratio was reported to be ∼(+)2 × 10^{-5} for the (1*R*,4*R*)-(+) enantiomer. This result was recently confirmed by Wang and Keiderling.[13] At the present time, the VCD of **2** in this region has not been reported.

For both B3PW91 and B3LYP, TZ2P calculations predict a large dipole strength and a positive anisotropy ratio of (1−2)

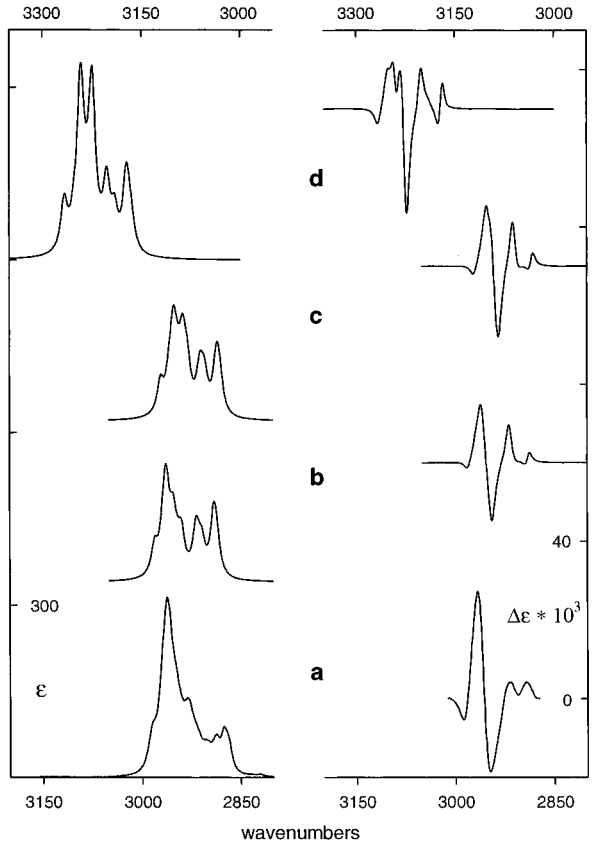

Figure 7. Experimental (a) and calculated (b−d) absorption and VCD spectra of **1**. The experimental spectrum and VCD spectra are in CCl_4 solution (0.02 M) at 1 cm^{-1} and 10 cm^{-1} resolution, respectively. The VCD spectrum is half the difference of the VCD spectra of (+)-**1** and (−)-**1**. Calculated spectra are (b) DFT/B3PW91/TZ2P; (c) DFT/B3LYP/TZ2P; (d) HF/SCF/TZ2P. $\gamma = 6$ cm^{-1} for all bands in (b−d). The lower frequency scale applies to (a).

$\times 10^{-5}$ for the (1*R*,4*R*)-(+) enantiomer of **1** (Table 1), in excellent agreement with experiment.

C−H Stretching Spectral Region. Experimental absorption and VCD spectra of **1** in the C−H stretching region are shown in Figure 7, together with spectra obtained from the calculated frequencies, dipole strengths, and rotational strengths given in Table 1. The experimental spectra are complex, due to the presence of 16 fundamentals in a narrow frequency range and, undoubtedly, significant contributions from nonfundamentals in this region. The B3PW91/TZ2P and B3LYP/TZ2P spectra are similar and exhibit substantial qualitative resemblance to the experimental spectra. However, the complexity of the spectra in this region precludes more detailed analysis.

Far-IR Spectral Region. An absorption spectrum of **1** in cyclohexane solution over the range 50−300 cm^{-1} has been reported by Polavarapu and Chen.[33] By comparison to the B3PW91/TZ2P calculation (Table 1), the bands at ∼120 and ∼300 cm^{-1} can be assigned to fundamentals 1 and 9, respectively. Bands at ∼245 and ∼265 cm^{-1} are probably due to fundamentals 5, 6, and 7. Attempts to observe circular dichroism in this region were unsuccessful.[33]

Basis Set Dependence. The results of DFT calculations for **1** and **2** at the 6-31G* basis set level are given in Tables 3 and 6 and Figures 8−11. The 6-31G* B3PW91 and B3LYP absorption and VCD spectra are qualitatively identical to the corresponding TZ2P spectra.

HF/SCF Calculations. TZ2P and 6-31G* calculations for **1** and **2** have also been carried out at the HF/SCF level. The results are given in Tables 1, 3, 4, and 6 and Figures 2, 4−6, and 8−11. As expected,[32] the HF/SCF spectra are shifted to higher frequencies relative to the DFT spectra. As with the DFT spectra, 6-31G* and TZ2P spectra are qualitatively identical. The HF/SCF and DFT/B3PW91 spectra exhibit considerable similarity. However, substantial differences exist, especially in the VCD spectra. The differences are most marked in the case of **1** for bands 24−29, 33, 35−40 and, in the case of **2**, for bands 30, 35, and 38. Where different, the HF/SCF spectra are in worse agreement with experiment.

TABLE 6: 6-31G* Calculations for Fenchone (2)[a]

	DFT								
	B3PW91			B3LYP			HF/SCF		
mode	*ν*	*D*	*R*	*ν*	*D*	*R*	*ν*	*D*	*R*
59	1848	373.7	−8.0	1832	368.3	−7.9	2029	480.2	−6.8
58	1552	18.7	−6.7	1557	14.9	−3.8	1683	12.3	−2.1
57	1535	28.9	−6.3	1542	21.9	−4.5	1664	17.8	−2.2
56	1528	26.0	7.2	1534	20.8	5.8	1659	13.7	1.6
55	1524	3.0	2.3	1530	0.8	−0.7	1649	5.3	−1.3
54	1520	17.6	−14.8	1526	14.6	−11.7	1646	6.6	−5.9
53	1516	18.9	−2.1	1523	10.3	0.9	1639	7.7	−1.3
52	1512	3.9	−0.9	1518	6.3	−4.0	1637	10.2	−4.3
51	1507	5.4	−0.5	1514	4.1	−0.3	1636	3.0	3.8
50	1502	2.6	0.2	1510	3.1	0.1	1630	2.5	−0.2
49	1436	22.1	−6.1	1443	20.8	−2.5	1573	13.8	−1.5
48	1435	18.2	2.3	1442	6.8	−0.1	1568	3.3	0.0
47	1413	15.4	−2.5	1421	9.1	−1.3	1551	6.5	−1.8
46	1376	8.4	−10.6	1372	8.3	−8.8	1505	16.9	−9.6
45	1360	11.0	7.5	1359	9.8	4.7	1490	13.3	6.7
44	1330	13.4	−5.7	1332	12.4	−3.9	1467	7.9	−4.1
43	1306	6.0	−1.1	1304	5.1	−1.4	1431	4.3	−0.9
42	1284	1.2	1.8	1286	2.2	2.8	1410	4.5	4.7
41	1278	4.3	0.0	1278	1.9	−1.6	1399	2.2	−2.5
40	1260	7.9	1.2	1256	8.0	0.1	1382	6.4	0.5
39	1249	10.0	−12.4	1248	10.7	−11.2	1356	11.0	−14.0
38	1229	0.8	0.3	1226	0.5	−1.8	1337	0.2	−2.2
37	1202	7.2	21.5	1199	9.4	22.6	1312	6.3	17.6
36	1190	5.8	1.8	1187	5.4	2.0	1301	7.0	1.3
35	1147	8.8	6.5	1141	8.2	3.0	1245	11.0	−1.0
34	1133	18.1	11.8	1134	14.9	9.0	1234	13.5	8.8
33	1097	3.6	7.2	1098	3.1	4.6	1195	5.2	13.8
32	1047	71.2	66.2	1048	44.0	60.6	1141	96.5	50.5
31	1040	116.2	−58.4	1037	107.5	−50.0	1130	26.0	−50.1
30	1021	11.0	−24.7	1023	12.4	−19.1	1109	9.6	−15.2
29	1013	21.2	−6.1	1014	48.2	−6.7	1100	26.4	−5.2
28	979	22.4	−0.9	972	25.5	−6.5	1051	21.8	−8.6
27	969	1.7	−2.4	968	1.4	−1.9	1044	1.3	−2.1
26	963	23.4	18.2	957	23.1	19.0	1032	14.6	15.9
25	949	46.0	−25.7	940	49.2	−20.9	1022	24.0	−15.6
24	910	2.3	11.5	900	2.7	10.6	971	1.3	8.9
23	906	1.6	0.7	895	0.8	0.9	958	2.0	0.4
22	849	2.5	−3.8	845	1.1	−4.1	920	1.5	−4.9
21	847	17.8	0.7	838	16.5	14.8	908	18.8	−2.6
20	836	12.8	3.3	834	13.3	−11.9	900	19.1	13.5
19	790	1.3	0.8	786	1.2	0.7	852	2.7	1.0
18	725	3.6	2.3	720	3.6	2.8	784	5.3	−2.1
17	663	11.5	6.9	659	10.5	6.5	713	1.4	3.2
16	600	4.9	−1.0	596	4.7	−1.2	640	1.7	0.0
15	522	18.9	6.2	521	18.1	6.1	563	29.9	7.1
14	509	15.9	−2.7	510	18.0	−2.2	546	25.7	−2.1
13	439	4.1	5.0	444	3.9	4.2	481	3.8	3.7
12	419	5.6	−5.6	420	6.1	−4.9	452	8.7	−4.8
11	372	3.9	3.8	373	3.7	3.4	398	2.8	3.0
10	325	2.3	6.3	327	2.0	5.5	351	1.9	4.7
9	298	5.1	−1.6	299	7.3	−1.5	322	11.2	−0.7
8	289	80.4	−2.5	292	78.7	−1.9	316	95.6	−2.3
7	256	7.9	−0.3	258	6.3	−0.2	281	5.0	−1.3
6	227	21.0	−2.1	228	21.1	−1.2	252	11.3	0.0
5	206	14.0	0.0	208	11.8	−1.0	230	16.3	−0.2
4	191	22.2	6.8	192	23.1	5.9	217	9.9	3.2
3	184	1.9	1.1	184	1.5	0.6	214	0.3	0.1
2	174	19.0	5.1	175	18.8	5.1	203	39.7	0.4
1	82	107.0	0.1	83	106.0	−0.1	93	126.2	−0.1

[a] Units as in Table 4.

Quantitative Accuracy. The quantitative accuracies of the TZ2P and 6-31G* calculations for **1** and **2** are assessed by comparison of the calculated and experimental frequencies, dipole strengths and rotational strengths as shown in Figures

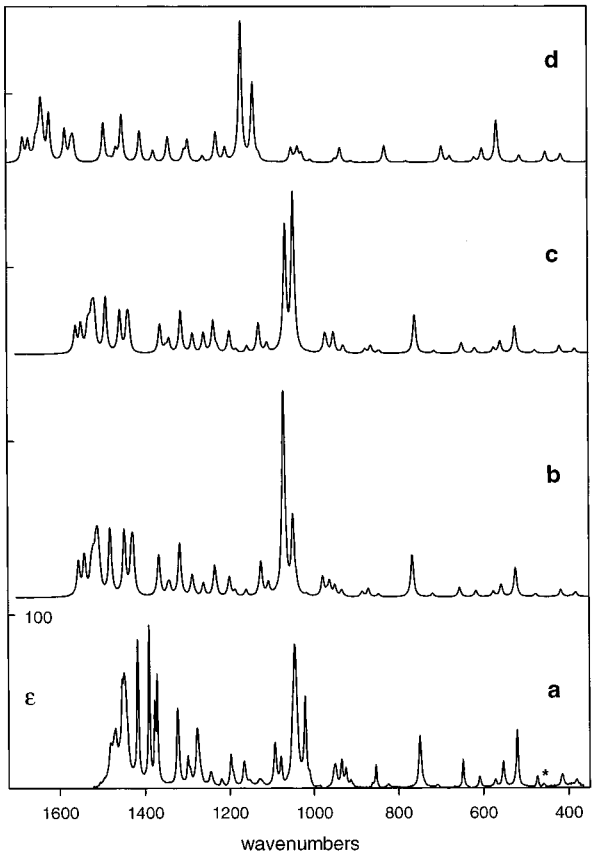

Figure 8. Experimental (a) and calculated (b−d) absorption spectra of **1**. The experimental spectrum is from Figure 1a (1525−840 and 680−365 cm^{-1} in CCl_4; 840−680 cm^{-1} in CS_2). Calculated spectra are (b) DFT/B3PW91/6-31G*; (c) DFT/B3LYP/6-31G*; (d) HF/SCF/6-31G*. $\gamma = 4$ cm^{-1} for all bands in (b−d). The asterisked band in (a) is not due to **1**.

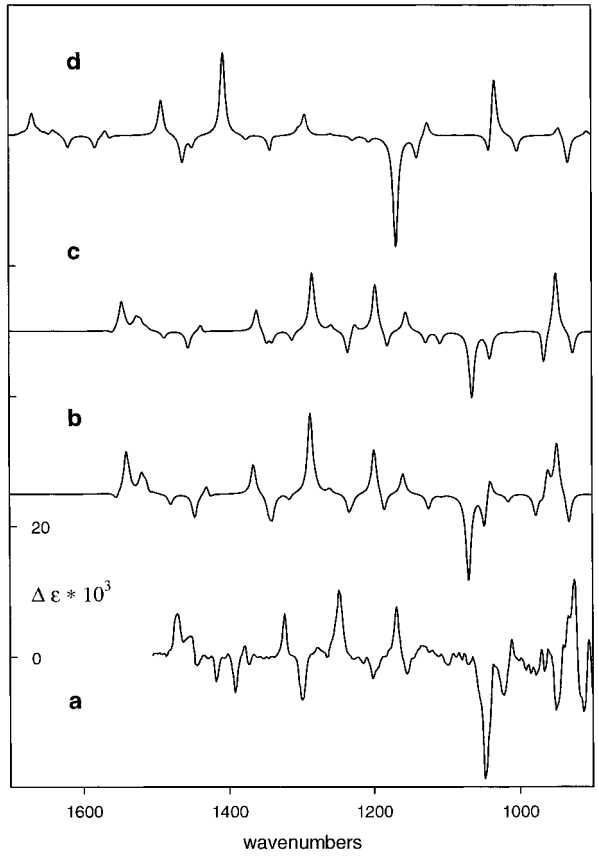

Figure 9. Experimental (a) and calculated (b−d) VCD spectra of **1**. The experimental spectrum is from Figure 3a. Calculated spectra are (b) DFT/B3PW91/6-31G*; (c) DFT/B3LYP/6-31G*; (d) HF/SCF/6-31G*. $\gamma = 4$ cm^{-1} for all bands in (b−d).

12−14. Figure 12 compares calculated and experimental frequencies. With the exception of frequencies below 600 cm^{-1}, all calculated frequencies are always greater than experimental frequencies. Overall, the percentage deviation increases with increasing frequency. The DFT/B3PW91 and DFT/B3LYP calculations are very similar in accuracy. The HF/SCF calculations are much less accurate. Percentage deviations are larger at the 6-31G* basis set level than at TZ2P. Figures 13 and 14 compare calculated and experimental dipole and rotational strengths. The superior accuracy of the DFT/B3PW91 calculations is apparent. With the exception of the dipole strengths of modes 31 and 32 of **2**, the agreement of both calculated and experimental dipole strengths and rotational strengths is excellent at both TZ2P and 6-31G* basis set levels. The DFT/B3LYP and HF/SCF calculations are both in poorer agreement with experiment.

The quantitative agreement with experiment of the DFT/B3PW91/TZ2P calculations is not perfect, of course. Errors remain in the calculations due to the neglect of solvent effects and anharmonicity, the inaccuracy of the B3PW91 functional and basis set incompleteness. Errors in the experimental dipole and rotational strengths are also undoubtedly significant and the rotational strengths are not normalized to 100% ee.

Discussion

Our results show that (1) hybrid functional DFT calculations of HFFs, APTs and AATs, and thence harmonic frequencies, dipole strengths, and rotational strengths, involving 400−500 basis functions are now feasible; (2) predicted spectra depend on the functional used and comparison of predicted and experimental spectra permits their relative accuracies to be assessed; (3) the basis sets 6-31G* and TZ2P yield qualitatively very similar results; (4) the B3PW91/TZ2P calculations are in best agreement with experiment and provide an unambiguous assignment of a large fraction of the fundamentals of **1** and **2**; only modes whose absorption and VCD are both very weak and groups of unresolved modes are not definitely assigned.

We have previously reported calculations of vibrational absorption and VCD spectra using DFT.[1,2,15,29,30,34,35] In our earliest calculations,[15,29,30,34,35] DFT HFFs and APTs were used, together with "semi-DFT" AATs. Semi-DFT AATs are distributed origin gauge AATs[17,18] in which DFT ATPs and HF/SCF "local" AATs are combined. As a result, absorption spectra were calculated more accurately than VCD spectra. Very recently, as a result of the development and implementation of techniques for calculating AATs using DFT,[1,2] full DFT calculations of VCD spectra have become possible. Results have been reported for *trans*-2,3-oxirane-d_2[1] and 6,8-dioxa[3.2.1]-bicyclooctane.[2] The present work constitutes an extension to larger molecules.

In our previous work we have compared the accuracies of vibrational spectra predicted using local, nonlocal (gradient-corrected) and hybrid functionals, specifically LSDA, BLYP, and B3LYP.[15,29,30,34,35] We have demonstrated the superiority of the hybrid functional B3LYP over LSDA and BLYP, a result consistent with other studies of other molecular properties.[32,36−42] However, we have not previously explored the variation of spectra with hybrid functional. At the present time, the original three-parameter Becke functional, B3PW91,[22] and two analogous functionals, B3LYP and B3P86,[43] are available in the GAUSSIAN program.[28] For a range of molecules B3PW91 and B3P86 have given extremely similar vibrational spectra.[44] In this work we have therefore examined the two functionals B3PW91 and B3LYP. Overall, the two functionals give

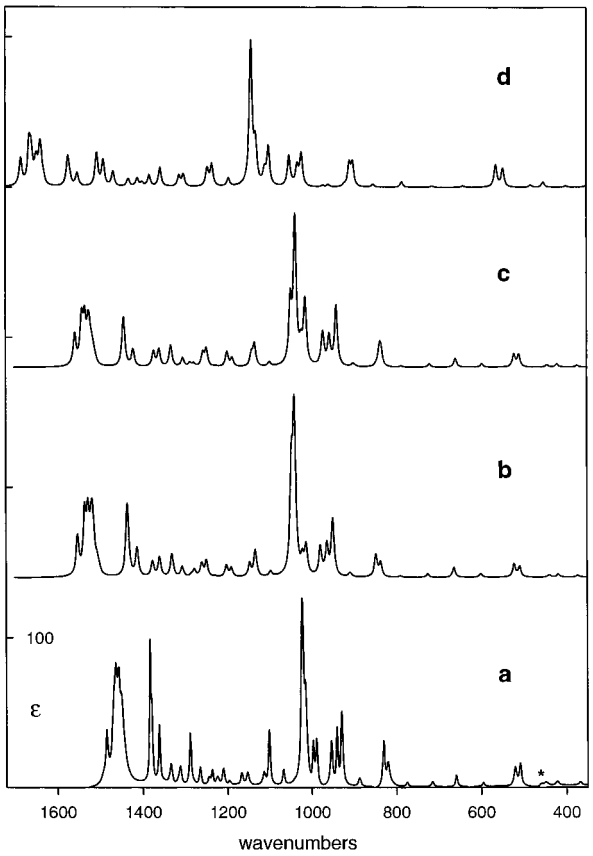

Figure 10. Experimental (a) and calculated (b−d) absorption spectra of **2**. The experimental spectrum is from Figure 1b (1525−860 and 690−350 cm^{-1} in CCl_4; 860−690 cm^{-1} in CS_2). Calculated spectra are (b) DFT/B3PW91/6-31G*; (c) DFT/B3LYP/6-31G*; (d) HF/SCF/6-31G*. $\gamma = 4$ cm^{-1} for all bands in (b−d). The asterisked band in (a) is not due to **2**.

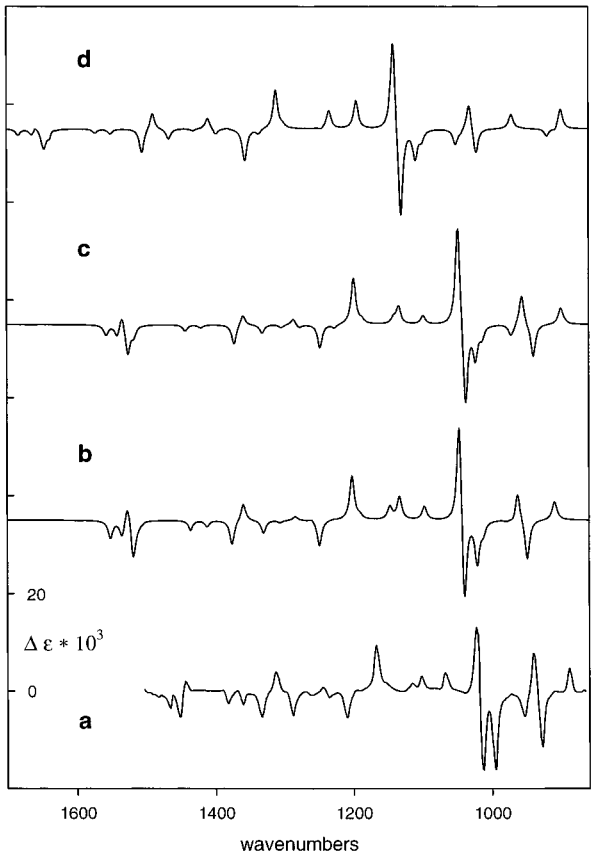

Figure 11. Experimental (a) and calculated (b−d) VCD spectra of **2**. The experimental spectrum is from Figure 3b. Calculated spectra are (b) DFT/B3PW91/6-31G*; (c) DFT/B3LYP/6-31G*; (d) HF/SCF/6-31G*. $\gamma = 4$ cm^{-1} for all bands in (b−d).

qualitatively very similar spectra. In a few spectral regions qualitative differences occur and B3PW91 is uniformly in better agreement with experiment. We conclude that B3PW91 is slightly more accurate than B3LYP for **1** and **2**. The generality of this result remains to be explored.

The ability of the B3PW91/TZ2P calculations to reproduce the experimental spectra of **1** and **2** is impressive. The accurate prediction of vibrational intensities requires accurate normal coordinates, which in turn requires accurate harmonic force fields. Further, the accuracy required increases with increasing density of vibrational states and, hence, molecular size. Even greater accuracy in the HFF is therefore required for **1** and **2** than for smaller molecules. The accuracy of the HFFs of **1** and **2** can be assessed from the accuracy of their predicted frequencies. The B3PW91/TZ2P frequencies are within 3% of experimental frequencies for fundamentals up to 58 (Figure 12). A significant fraction of the difference is attributable to anharmonicity; harmonic frequencies probably differ by 1−2%.[32] This high accuracy in the HFFs is the reason for the excellent agreement of predicted and experimental spectra.

At the same time, it must be inferred that anharmonicity does not substantially perturb the experimental spectra, since otherwise harmonic calculations would not be able to reproduce experimental spectra. The same must be concluded with regard to solvent effects, which are present in the experiments but not in the calculations.

The accuracy of the DFT calculations reflects the substantial inclusion of correlation in the density functionals. HF/SCF calculations do not include correlation, by definition, and are intrinsically limited to a lower level of accuracy. The HF/SCF

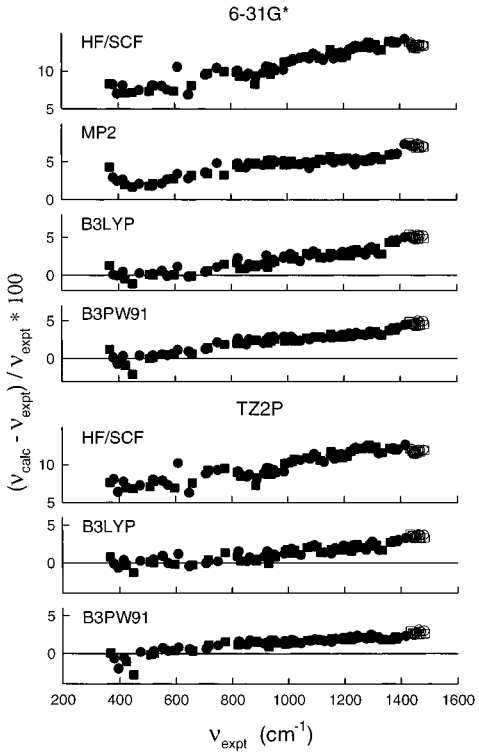

Figure 12. Comparison of calculated and experimental frequencies for **1** (●) and **2** (■). MP2 calculations are from prior work.[45] ○ and □ are modes 58−51 and 58−50 of **1** and **2** respectively.

calculations on **1** and **2** demonstrate the importance of correlation to the accurate prediction of vibrational spectra.

We have previously carried out calcuations for **1** and **2** at the 6-31G* basis set level using MP2 HFFs and APTs and

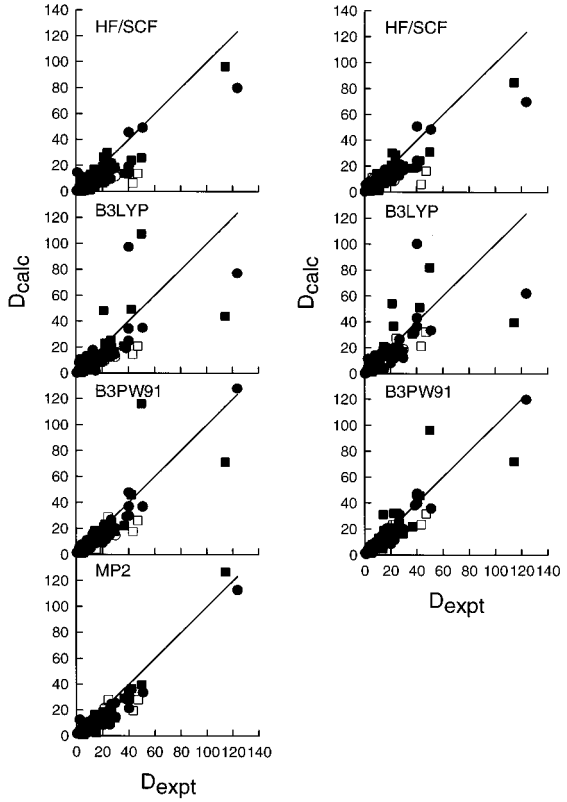

Figure 13. Comparison of calculated and experimental dipole strengths for **1** (●) and **2** (■). The left-hand column is for 6-31G* calculations; the right-hand column is for TZ2P calculations. MP2 calculations are from prior work.[45] ○ and □ are modes 58−51 and 58−50 of **1** and **2**, respectively.

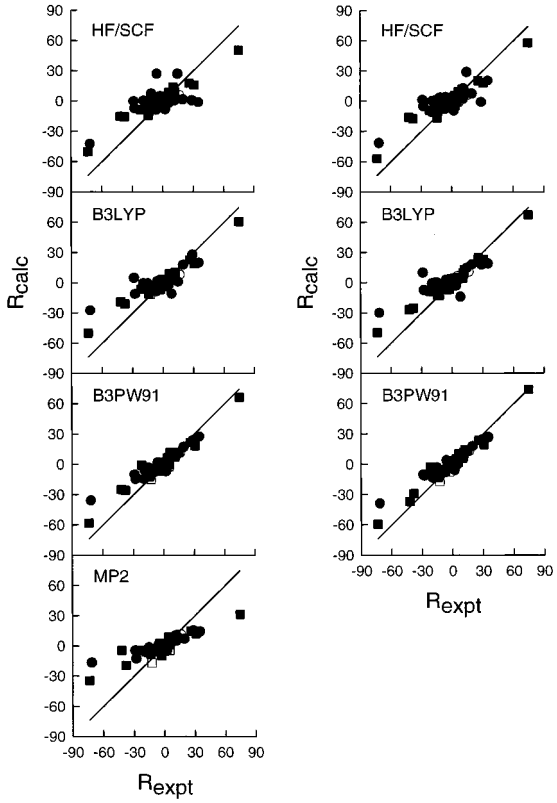

Figure 14. Comparison of calculated and experimental rotational strengths for **1** (●) and **2** (■). The left-hand column is for 6-31G* calculations; the right-hand column is for TZ2P calculations. Experimental rotational strengths are not normalized to 100% ee. MP2 calculations are from prior work.[45] ○ and □ are modes 58−51 and 58−50 of **1** and **2**, respectively.

"semi-MP2" AAT's.[14,45] These results are included in Figures 12−14. MP2 frequencies are somewhat less accurate than DFT/B3PW91 and DFT/B3LYP frequencies, but much more accurate than HF/SCF frequencies. MP2 dipole strengths compare favorably with DFT/B3PW91 dipole strengths: in particular, the dipole strengths of modes 31 and 32 of **2** are more successfully reproduced. MP2 rotational strengths conversely appear to be less accurate than DFT/B3PW91 values. This is not unexpected since the MP2 rotational strengths do not include correlation to the same degree and the "local" AATs were calculated using field-independent basis sets.

The work reported here can be extended and improved upon in a number of ways. The frequency ranges of both absorption and VCD spectroscopies can be extended to encompass all fundamentals of **1** and **2**. The sensitivity and resolution of VCD spectra can be improved, permitting weaker bands to be more definitively identified. Both absorption and VCD spectra can be obtained under higher resolution conditions, e.g., using matrix isolation techniques, permitting overlapping bands (such as 51−56 and 60−75 in **1** and 50−57 and 60−75 in **2**) to be more clearly separated. On the theoretical side, further improvements in density functionals are expected to provide more accurate predictions of absorption and VCD spectra.

Conclusion

If *ab initio* quantum chemistry can successfully predict the vibrational spectra of molecules of known structure, it provides a reliable basis for the characterization of molecules of unknown structure. Our results for camphor and fenchone document the accuracy of the *ab initio* DFT methodology, implemented at the harmonic level of approximation and using state-of-the-art density functionals in the case of molecules of substantial size and complexity. It is clear that when basis sets as large as 6-31G* or larger are employed, harmonic DFT calculations using hybrid functionals are of useful accuracy. In particular, the calculations of VCD spectra are certainly of sufficient accuracy to permit the determination of absolute configuration. This is an important development for the application of VCD spectroscopy to the determination of the sterochemistry of chiral molecules.

Acknowledgment. We are grateful to NIH and NSF for support of research on VCD at USC, to the San Diego Supercomputer Center for CRAY time, and to IBM for a SUR grant to USC.

References and Notes

(1) Cheeseman, J. R.; Frisch, M. J.; Devlin, F. J.; Stephens, P. J. *Chem. Phys. Lett.* **1996**, *252*, 211.
(2) Stephens, P. J.; Ashvar, C. S.; Devlin, F. J.; Cheeseman, J. R.; Frisch, M. J. *Mol. Phys.* **1996**, *89*, 579.
(3) Nafie, L. A.; Keiderling, T. A.; Stephens, P. J. *J. Am. Chem. Soc.* **1976**, *98*, 2715.
(4) Keiderling, T. A.; Stephens, P. J. *Chem. Phys. Lett.* **1976**, *41*, 46.
(5) Stephens, P. J.; Clark, R. In *Optical Activity and Chiral Discrimination*; Mason, S. F., Ed.; D. Reidel: Dordrecht, 1979; Chapter X, pp. 263−287.
(6) Nafie, L. A.; Diem, M.; Vidrine, D. W. *J. Am. Chem. Soc.* **1979**, *101*, 496.
(7) Nafie, L. A.; Diem, M. *Acc. Chem. Res.* **1979**, *12*, 296.
(8) Nafie, L. A. In *Vibrational Spectra and Structure*; Durig, J. R., Ed.; Wiley: New York, 1981; Vol. 10, Chapter 2, pp 153−225.
(9) Nafie, L. A. In *Advances in Infrared and Raman Spectroscopy*; Clark, R. J. H., Hester, R. E., Ed.; Wiley: New York, 1984; Vol. 11, Chapter 2, pp 49−93.
(10) Yang, W. J.; Griffiths, P. R.; Kemeny, G. J. *Appl. Spectrosc.* **1984**, *38*, 337.
(11) Nafie, L. A. In *Advances in Applied FTIR Spectroscopy*; MacKenzie, M. W., Ed.; Wiley: New York, 1988; pp 67−104.
(12) Polavarapu, P. L.; Chen, G. C.; Weibel, S. *Appl. Spectrosc.* **1994**, *48*, 1224.

(13) Wang, B.; Keiderling, T. A. *Appl. Spectrosc.* **1995**, *49*, 1347.
(14) Devlin, F. J.; Stephens, P. J. *J. Am. Chem. Soc.* **1994**, *116*, 5003.
(15) Stephens, P. J.; Devlin, F. J.; Ashvar, C. S.; Chabalowski, C. F.; Frisch, M. J. *Faraday Discuss.* **1994**, *99*, 103.
(16) Stephens, P. J. *J. Phys. Chem.* **1985**, *89*, 748.
(17) Stephens, P. J. *J. Phys. Chem.* **1987**, *91*, 1712.
(18) Stephens, P. J.; Jalkanen, K. J.; Amos, R. D.; Lazzeretti, P.; Zanasi, R. *J. Phys. Chem.* **1990**, *94*, 1811.
(19) Johnson, B. G.; Frisch, M. J. *Chem. Phys. Lett.* **1993**, *216*, 133.
(20) Johnson, B. G.; Frisch, M. J. *J. Chem. Phys.* **1994**, *100*, 7429.
(21) Becke, A. D. *J. Chem. Phys.* **1993**, *98*, 1372.
(22) Becke, A. D. *J. Chem. Phys.* **1993**, *98*, 5648.
(23) Devlin, F. J.; Stephens, P. J.; Cheeseman, J. R.; Frisch, M. J. *J. Am. Chem. Soc.* **1996**, *118*, 6327.
(24) Devlin, F. J.; Stephens, P. J. *Appl. Spectrosc.* **1987**, *41*, 1142.
(25) Devlin, F. J.; Stephens, P. J.; Cheeseman, J. R.; Frisch, M. J. Submitted for publication.
(26) Kawiecki, R. W.; Devlin, F. J.; Stephens, P. J.; Amos, R. D.; Handy, N. C. *Chem. Phys. Lett.* **1988**, *145*, 411.
(27) Kawiecki, R. W.; Devlin, F. J.; Stephens, P. J.; Amos, R. D. *J. Phys. Chem.* **1991**, *95*, 9817.
(28) Frisch, M. J., et al. *GAUSSIAN 95*, Development Version; Gaussian Inc.: Pittsburgh, PA, 1995.
(29) Stephens, P. J.; Devlin, F. J.; Chabalowski, C. F.; Frisch, M. J. *J. Phys. Chem.* **1994**, *98*, 11623.
(30) Devlin, F. J.; Finley, J. W.; Stephens, P. J.; Frisch, M. J. *J. Phys. Chem.* **1995**, *99*, 16883.
(31) Hehre, W. J.; Radom, L.; Schleyer, P. R.; Pople, J. A. *Ab Initio Molecular Orbital Theory*; Wiley: New York, 1986.
(32) Finley, J. W.; Stephens, P. J. J. *Mol. Struct. (THEOCHEM.)* **1995**, *357*, 225.
(33) Polavarapu, P. L.; Chen, G. C. *Appl. Spectrosc.* **1994**, *48*, 1410.
(34) Stephens, P. J.; Devlin, F. J.; Ashvar, C. S.; Bak, K. L.; Taylor, P. R.; Frisch, M. J. In *Chemical Applications of Density Functional Theory*; Laird, B. B.; Ross, R. B.; Ziegler, T. ACS Symposium Series 629; American Chemical Society: Washington, DC, 1996; Chapter 7, p 105.
(35) Ashvar, C. S.; Devlin, F. J.; Bak, K. L.; Taylor, P. R.; Stephens, P. J. *J. Phys. Chem.* **1996**, *100*, 9262.
(36) Wong, M. W. *Chem. Phys. Lett.* **1996**, *256*, 391.
(37) Scott, A. P.; Radom, L. *J. Phys. Chem.* **1996**, *100*, 16502.
(38) De Proft, F.; Martin, J. M. L.; Geerlings, P. *Chem. Phys. Lett.* **1996**, *250*, 393.
(39) Cheeseman, J. R.; Trucks, G. W.; Keith, T. A.; Frisch, M. *J. Chem. Phys.* **1996**, *104*, 5497.
(40) Foresman, J. B.; Frisch, A. E. *Exploring Chemistry with Electronic Structure Methods*, 2nd ed.; Gaussian, Inc.: Pittsburgh, PA, 1996.
(41) Frisch, M. J.; Trucks, G. W.; Cheeseman, J. R. In *Recent Developments and Applications of Modern Density Functional Theory*; Seminario, J. M., Ed.; Elsevier: New York, 1996; Chapter 18, pp 679−707.
(42) Curtiss, L. A.; Raghavachari, K.; Redfern, P. C.; Pople, J. A. *J. Chem. Phys.* **1997**, *106*, 1063.
(43) Based on the correlation functional of: Perdew, J. P. *Phys. Rev. B*, **1986**, *33*, 8822.
(44) Cheeseman, J. R.; Frisch, M. J.; Devlin, F. J.; Stephens, P. J., to be published.
(45) Devlin, F. J.; Stephens, P. J., unpublished calculations.